CARD11 gain of function upregulates BCL2A1 and promotes resistance to targeted therapies combination in B-cell lymphoma

Salomé Decombis, Céline Bellanger, Yannick Le Bris, Candice Madiot, Jane Jardine, Juliana Carvalho Santos, Delphine Boulet, Christelle Dousset, Audrey Menard, Charlotte Kervoelen, et al.

CARD11 gain of function upregulates BCL2A1 expression and promotes resistance to targeted therapies combination in B-cell lymphoma

Salomé Decombis[1]*, Céline Bellanger[1]*, Yannick Le Bris[2], Candice Madiot[1], Jane Jardine[1], Juliana Carvalho Santos[3], Delphine Boulet[1], Christelle Dousset[1], Audrey Menard[2], Charlotte Kervoelen[4], Élise Douillard[1], Philippe Moreau[2], Stéphane Minvielle[1], Agnès Moreau-Aubry[1], Benoit Tessoulin[2], Gael Roué[3], Nicolas Bidère[1], Steven Le Gouill[5], Catherine Pellat-Deceunynck[1] and David Chiron[1]**

[1] Nantes Université, Inserm, CNRS, Université d'Angers, CRCI[2]NA, Nantes - France
[2] Nantes Université, CHU de Nantes, INSERM, CNRS, Université d'Angers, CRCI[2]NA, Nantes - France
[3] Lymphoma Translational Group, Josep Carreras Leukaemia Research Institute (IJC), Badalona.
[4] Therassay (Onco-Hemato) Core Facility, Nantes Université, Capacités, Nantes, France
[5] Institut Curie, Paris, France

*equal contribution

** Corresponding author:

Tel: +33 228080266

Address: 8 quai Moncousu, 44007 Nantes, France

E-mail: david.chiron@univ-nantes.fr

Disclosure

No potential conflicts of interest were disclosed by the authors

Key words: Mantle Cell lymphoma, Ibrutinib, Venetoclax, scRNA-seq, MALT1-inhibitors

Abstract

Strategy combining targeted therapies is effective in B-cell lymphomas such as mantle cell lymphoma (MCL), but acquired resistances remain a recurrent issue. Herein, we performed integrative longitudinal genomic and single-cell RNA-seq analyses of MCL patients treated with targeted therapies against CD20, BCL2 and BTK (i.e., OAsIs trial). We revealed the emergence of subclones with a selective advantage against OAsIs combination *in vivo* and showed that resistant cells were characterized by BCR-independent overexpression of NFkB1 target genes, especially due to CARD11 mutations. Functional studies demonstrated that CARD11 gain of function not only resulted in BCR independence, but also directly increase the transcription of the antiapoptotic *BCL2A1*, leading to venetoclax and OAsIs combination resistance. Based on the transcriptional profile of OAsIs-resistant subclones, we designed a 16-gene resistance signature that was also predictive for MCL patients treated with conventional chemotherapy, underlying a common escape mechanism. Among druggable strategies to inhibit CARD11-dependent NFkB1 transduction, we evaluated the selective inhibition of its essential partner MALT1. We demonstrated that MALT1 protease inhibition led to the reduction of genes involved in OAsIs resistance, including *BCL2A1*. Consequently, MALT1 inhibition induced synergistic cell death in combination with BCL2 inhibition, irrespective of CARD11 mutational status, both *in vitro* and *in vivo*. Taken together our study identified mechanisms of resistance to targeted therapies and provided a novel strategy to overcome resistance in aggressive B-cell lymphoma.

- BCR-independent NFKB1 identified as a mechanism of MCL relapse *in vivo*
- CARD11/NFKB1/BCL2A1 axis is counteracted by MALT1/BCL2 dual targeting

Introduction

Over the past decade, efforts to characterize the molecular profiles of Mantle Cell Lymphoma (MCL) cells, as well as the multiple interactions that occur in their malignant ecosystems, have identified tumor vulnerabilities[1,2]. Among them, elevated CD20 expression[3], imbalance in the Bcl2 family[4], and constitutive BCR signaling[5] have emerged as promising druggable pathways. Indeed, anti-CD20 Abs (i.e. rituximab), Bcl2 inhibitors (i.e. venetoclax), and BTK inhibitors (i.e. ibrutinib) have shown great promise as single agents[6,7] or in combination with chemotherapy[8,9].

Nevertheless, heterogeneity coupled with tumor cell plasticity significantly limits the long-term efficacy of targeted monotherapies[10,11]. As a result, multiple mechanisms of resistance arising from both mutations and microenvironmental cues have been described. For example, the selection of MCL cells with Bcl2 amplicon loss has been observed during venetoclax treatment[12], and the microenvironment-dependent expression of alternative anti-apoptotic proteins has been described as a major means of escape[13,14]. Similarly, despite a strong dependence on BCR-dependent NFκB activation, resistance to BTK inhibition rapidly emerges in MCL. Indeed, in addition to rare on-target mutations[15], mutational or microenvironment-dependent activation of the alternative NFκB pathway, as well as metabolic reprogramming, have been reported in ibrutinib-resistant cells[16,17].

To limit tumor adaptability, mechanism-based combinations of targeted therapies are being designed. We previously demonstrated that pre-treatment with obinutuzumab, an anti-CD20 antibody[13], and ibrutinib[18] was able to counteract microenvironment-dependent resistance to venetoclax in MCL, mostly through the down-regulation of NFκB-dependent BCLxL expression. This rationale was involved in the design of the OAsIs trial, which consists of a sequential combination of obinutuzumab and ibrutinib followed by venetoclax in MCL patients. This triple "chemo-free" combination was well tolerated and led to a complete response rate of 67% and 86.6% in relapsed and untreated patients, respectively[19]. Nevertheless, despite these high initial response rates, nearly one-third of the patients progressed or rapidly relapsed. Here, by combining comprehensive genomics and single-cell transcriptomics, we

established a novel signature of *in vivo* resistance and deciphered the molecular mechanisms underlying tumor escape. Based on the mechanisms we discovered, we performed functional studies to identify therapeutic vulnerabilities that could be exploited in order to overcome lymphoma resistance.

Methods

Patient samples cohort

Samples were collected from peripheral blood (PB), bone marrow (BM) or lymph nodes (LN) after obtaining informed consent from MCL patients (REFRACT-LYMA cohort; ethical approval GNEGS-2015-09-1317) and in accordance with the Declaration of Helsinki. Characteristics of patients who participated in the OAsIs trial (NCT02558816) were summarized in Supp Table S1.

Deep DNA sequencing

All samples from patients enrolled in the OAsIs trial available at our institution and containing at least 5% of circulating MCL cells (CD19+ CD5+) were used for comprehensive genomics. DNA was extracted from CD19+ MCL cells (17 samples from 14 patients) previously enriched using anti-human CD19-conjugated magnetic beads (Miltenyi®). A panel including 49 genes and 170 exons from the 9p21 region was designed to identify recurrent mutations and copy number variations (CNV), based on hits described in the literature for their role in lymphomagenesis (Supp Table S2). Probes were produced by Integrated DNA Technologies (IDT®).

Single-cell RNA-sequencing

Seven BM samples from 6 patients included in the OAsIs trial were analyzed at the single cell resolution. Briefly, live MCL cells were first enriched by Ficoll-Paque Plus and anti-human CD19 magnetic beads. Depletion of human erythroid precursors and erythrocytes was then performed using CD235a (Glycophorin-A) magnetic beads. 15,000 cells from the resulting suspensions were loaded on a Chromium controller to generate single-cell partitions following the manufacturer's protocol (10X genomics).

scRNA-seq libraries were constructed using the Chromium Next GEM Single Cell 3' GEM, Library & Gel Bead Kit v3.1 and sequenced using the NovaSeq 6000 system (Illumina). Overall, 88 034 cells were sequenced with a median of 14 805 per sample and an average of

50 686 reads per cell. Data processing and bioinformatics analysis are detailed in the supplemental Methods section.

Chick embryo chorioallantoic membrane (CAM) model

Fertilized white Leghorn chicken eggs were purchased from Granja Santa Isabel, S. L. (Córdoba, Spain) and incubated for 9 days at 37 °C with 55% humidity. At day 9 of their embryonic development, a window of an approximate 2 cm-diameter was drilled on top of the air chamber of the eggshell. Then, half million DFBL-44685v2 CARD11^{D230N} PDX MCL cells were suspended in 25 µL RPMI medium containing 10% FBS and 100 U/mL penicillin and streptomycin and 25 µL Matrigel. The mix was incubated for 15 min at 37 °C and subsequently implanted into the CAM of each egg. 250 nM of JNJ-67856633 (day 12 and 13), 2 nM of venetoclax (day 13) or both were administered topically on the tumor-bearing CAMs. Seven days post-implantation (day 16), chick embryos were sacrificed by decapitation. Tumors were excised and carefully weighed to determine their mass.

Additional methods are detailed in the supplemental Methods section and Supp Table S3 or have been previously described[20].

Data-sharing statement

RNA-sequencing datasets are publicly available in the Gene Expression Omnibus. All other datasets analyzed during the current study are available from the corresponding author on reasonable request.

Results

Selective advantage of CARD11^{GOF} mutated cells under OAsIs combination

Fresh tumor tissues from MCL patients enrolled in the OAsIs trial were collected and comprehensive genomic analysis (SNV/CNV, n=17) was performed on CD19+ MCL cells (Fig.1A; Supp Table S1-2). The most frequently altered genes at inclusion included *ATM* (6/12), *TP53* (5/12), and *KMT2D* (5/12) (Fig.1B, Supp Table S2). Only *CARD11* mutations were enriched at relapse (n=3/5, Fisher t=0.01), suggesting a selective advantage of *CARD11* mutated cells under OAsIs therapy (Fig.1C).

This was further confirmed by the longitudinal analysis of patient MCL34 samples at the time of diagnosis (Diag), before inclusion in the OAsIs trial (incl.), and at relapse (Rel). In contrast to a poor response to first-line chemotherapy (R-CHOP, stable disease), he achieved a complete molecular response before relapsing after 12 months of OAsIs treatment[19]. While most hits were similar across the samples, we observed at relapse the emergence of a gain-of-function (GOF) *CARD11* mutation (G123S, latch domain)[21,22] and the downfall of a loss-of-function (LOF) *TRAF2* variant (C49F, ring domain[23], Fig.1D, Supp Table S2). Indeed, while *CARD11*^{G123S} MCL cells remained discrete after first-line treatment, they made up the majority of the tumor after OAsIs (Fig.1E). Of note, a deeper analysis of the G123 position revealed the presence of few c.367G>A reads before treatment (G123S frequency = 0.12 % at Diag, 0.19 % at incl.), confirming the hypothesis of selection, under OAsIs, of a rare subclone already present at diagnosis (Supp Table S4). Regarding *CARD11* mutations found in other OAsIs relapse biopsies, one was at the same position (G123D, MCL24) and another was located in the Coiled-coil (CC) domain (R235Q, MCL40), both of which leading in GOF[21,24]. Although we were unable to collect samples at OAsIs inclusion for these patients, paired analysis at diagnosis vs. OAsIs relapse showed an increased frequency of CARD11 mutated cells at relapse. (R235Q frequency: 31 and 48 %, respectively) (Supp Fig.S1). Finally, we detected *CARD11* mutations in 4 additional MCL patients from our local cohort (Refract-Lyma, n=48 sequenced), including 2 additional G123S mutants, suggesting that mutations at position G123 are not infrequent in MCL (Fig.1F, Supp Table S4).

Both *TRAF2* LOF and *CARD11* GOF have been reported as being involved in ibrutinib resistance, inducing BCR-independent NFκB2 and NFκB1 constitutive activity, respectively[25,26]. To understand the selective advantage of *CARD11* GOF in MCL under OAsIs, we performed a transcriptional analysis at the single-cell resolution of the patient MCL34 samples, before and at OAsIs relapse.

Longitudinal single-cell analysis uncovered a minor OAsIs-resistant subpopulation

We were able to sequence 4,860 BM MCL cells before OAsIs (incl.), and 5,345 cells at relapse (Rel) (Supp Fig.S2A). We observed an elevated NIK_NFκB2 transcriptional signature[27] at inclusion ($p<0.0001$), consistent with the functional consequences of the *TRAF2* LOF mutation observed in this sample (Fig.2A). By contrast, cells from the sample collected at relapse displayed higher NFκB1 and BCR signatures[27] ($p<0.0001$), consistent with the acquired *CARD11* GOF mutation (Fig.2A). We did not observe transcriptional modulation of the OAsIs targets (Supp Fig.S2B).

Unsupervised clustering of these longitudinal samples was performed to segregate the cells according to their transcriptional profile. Seven distinct clusters were identified, 2 of them being common at inclusion and relapse (clusters #4 and #5, Fig.2B). The cell-cycle signature analysis highlighted a proliferative heterogeneity among the clusters, clusters #3 and #4 brought together cycling MCL cells (44% and 85%, respectively, Fig.2C). Inference of the cell-cycle transcriptional program reassigned cycling cells to their quiescent counterpart clusters (Supp Fig.S2C), and hierarchical clustering highlighted a close transcriptional proximity between clusters #1 and #2 (incl.), as well as between clusters #6 and #7 (Rel.) (Supp Fig.S2D). Finally, single-cell trajectory analysis identified a small number of cells from the inclusion sample, which belonged to cluster #5, within the branches that contributed to the relapse, suggesting that cells belonging to this minor cluster were at the initiation of the relapse process (Fig.2D).

Functional annotation of each cluster's transcriptional signature confirmed enrichment of the cell-cycle program (#3 and #4), and highlighted increased transcriptional and translational

activity at relapse (#6 and #7). Enriched activity of the transcription factors NFκB1 and RELA were predicted at relapse (#5 and #6 / #7, $p<5x10^{-5}$), suggesting the central role of this transcriptional program in OAsIs resistance (Fig.2E). Altogether, we identified a minor subclone (cluster#5 187/4,860 cells at inclusion), before OAsIs therapy, that was resistant *in vivo*, survived upon treatment (393/5,345 cells at relapse), and was at the initiation of the clusters exclusively detected at relapse (#6 and #7). All relapse clusters were characterized by elevated NFκB1/RELA activity, which was consistent with the *CARD11* GOF mutation previously identified.

A 16-gene signature characteristic of OAsIs-resistant cells and associated with poorer outcome in MCL

We further focused our analysis on the NFκB1-related transcriptional signature characteristic of the OAsIs-resistant cluster #5 (n=742 genes, Fig. 2E, Supp Table S5), and assessed it at single-cell resolution in additional samples from 5 patients enrolled on OAsIs (Supp Fig.S3A). Unsupervised clustering highlighted intra-tumoral heterogeneity in all the samples, with 4 to 5 clusters identified in each case (Supp Fig.S3B), all of them displayed expression of the OAsIs targets, with the exception of CD20 loss in all the cells from the refractory patient MCL10 (Supp Fig.S3C). Proliferating clusters (Supp Fig.S3D) were inferred to limit the impact of heterogeneous proliferation in further analysis (Supp Fig.S4A).

We then observed that the OAsIs-resistant cluster#5 signature was significantly more elevated in refractory patients when compared to responders ($p<0.001$, Fig.3A, upper panel). This signature score was homogeneously elevated across the cellular clusters in non-responders and low for long-term responders (Supp Fig.S4B). By contrast, the score was significantly more elevated in one cluster from the patient who rapidly relapsed after initial PR (MCL12, cluster#4), as previously seen for MCL34 (cluster#5) (Fig.3A, lower panel).

We further designed the MCL_R16 signature composed of 16 top genes upregulated in OAsIs-resistant cluster #5 (MCL34, Fig.3B, Supp Table S5). Like the full resistance signature, the MCL_R16 signature was significantly more elevated in clusters #5 of MCL34 and #4 of

the MCL12 at inclusion, as well as after OAsIs relapse (Fig.3C, Supp Fig.S4C). The MCL_R16 signature partially overlapped and significantly correlated with previously described BCR and NFκB1 signatures (Supp Fig.S4D-E). Akin to all these signatures[27], MCL_R16 was significantly higher in MCL lymph nodes when compared to peripheral blood ($p<0.0001$) (Supp Fig.S4F), in line with the previously described increased resistance in MCL protective niches[13,28].

To investigate whether this resistance profile could be extended to other regimen, we computed the MCL_R16 score in gene expression data from MCL patients previously treated with chemotherapy (R-CHOP, n=122). Patients having a high MCL_R16 score (upper tercile) had significantly lower OS, the median survival time being 17.3 months for patients with a high MCL_16R score compared to 53.8 months for others ($p<0001$) (Fig.3D, upper panel). This observation was confirmed with an intensive regimen (Lyma-trial, n=99), in which patients with a higher MCL_R16 score had significantly shorter PFS (51 months vs. not reached, $p=0.028$) (Fig.3D, lower panel) and OS ($p=0.042$) (Supp Fig.S4G). While the proliferation score was also a strong predictor of clinical response, previously described BCR and NFκB signatures were not associated with OS or PFS (Fig.3D, Supp Fig.S4G).

BCL2A1 is frequently expressed in MCL and triggered resistance by buffering BH3-only proteins.

Among the top genes associated with OAsIs resistance (Fig.3B), *BCL2A1,* an anti-apoptotic member of the Bcl-2 family, has previously been described as a major venetoclax resistance factor[12,29,30]. In accordance with the MCL_R16 signature pattern, the *BCL2A1* RNA level was: 1) significantly higher at relapse compared to inclusion ($p<0.0001$) (Fig.4A); 2) especially elevated in non-responders (MCL10 and MCL24) (Supp Fig.S5A); and 3) enriched in a specific cluster of cells in the 2 patients who experienced rapid relapse after initial response (cluster #5 of MCL34 and #4 of MCL12) (Supp Fig.S5B). Frequent expression of *BCL2A1* was observed in PB MCL samples (n=63), whereas 3 out of 7 MCL cell lines displayed low levels (Fig.4B). This pattern of expression was further confirmed at the protein level in cell

lines (Supp Fig. S5C) and primary cells, including OAsIs-resistant cells (BCL2A1^{high}, MCL24) and OAsIs-sensitive cells (BCL2A1^{low}, MCL36, Fig.4C).

To address the impact of BCL2A1 expression in the OAsIs response, we carried out further functional assays. BCL2A1 downregulation sensitized BCL2A1^{high} SP53 and OCILY3 resistant cells to venetoclax (Supp Fig.S5D-E). Consistently, ectopic BCL2A1 expression resulted in a dramatic loss of sensitivity to selective BCL2 inhibition (LD_{50} venetoclax in Mino_ct = 25 nM vs. Mino_A1 > 100 nM) and to the OAsIs combination (LD_{50} Mino_ct = 6.25 vs. Mino_A1 > 100 nM) (Fig.4D, Supp Fig.S5F). As observed in Mino cells, the BCL2A1^{high} MCL cells from the refractory MCL10 patient were more resistant to the combination *ex vivo* than the MCL cells from responding MCL7 and MCL12 patients (Supp Fig.S5G).

We then performed dynamic BH3-profiling using the BCL2A1-specific peptide FS2[31]. We first observed that cytochrome-c release was not significantly increased in the presence of FS2 at baseline, suggesting that MCL cells were not primed on BCL2A1 (Fig.4E). By contrast, pre-treatment with venetoclax in venetoclax-sensitive Mino cells (LD_{50} =25 nM), or with a combination of BH3-mimetics in venetoclax-resistant SP53 cells (LD_{50} >2500 nM), resulted in elevated priming to BCL2A1 ($p<0.001$, 48% and 87% of cytochrome-c release, respectively, Fig.4E). These results suggest that BCL2A1 was able to capture back pro-apoptotic BH3-only released upon the targeting of other anti-apoptotic members of the Bcl2-family, resulting in diminished apoptosis induction (Supp Fig.S5H-I). Finally, we observed that BCL2A1 protein expression increased upon venetoclax treatment *in vitro* (Supp Fig.S5J), consistent with its stabilization once it is in complex with BH3-only proteins[30]. Overall, our results highlighted that elevated expression of BCL2A1 could be involved in resistance to selective BCL2-targeted monotherapy but also in combination, such as OAsIs.

BCR-dependent expression of BCL2A1 is disrupted by BTK inhibition, resulting in cell death synergy in combination with BCL2 inhibition.

We observed a strong correlation between *BCL2A1* RNA level and the BCR signature in MCL cells ($r= 0.5$, $p<0.0001$; Fig.5A, Supp Fig.S6A). In line with a BCR-dependent

expression, *BCL2A1* was induced 3h after IgM engagement (median increase of 5.25-fold, n= 5, p<0.05, Fig.5B). This was further confirmed at the protein level (Fig.5C).

Accordingly, *BCL2A1* was inhibited by ibrutinib in all BCL2A1+ cell lines (median reduction: 34%, n=4, p<0.05), in a manner similar to the sensitive BCR activation marker *CD83*[32], but unlike other anti-apoptotic Bcl2 family proteins (Fig.5D). Consequently, ibrutinib reduced the BCL2A1 protein level (Supp Fig.S6B), leading to synergistic apoptosis when associated with venetoclax in BCL2A1+, but not in BCL2A1- cells (mean synergy score: 17 vs. 1) (Fig.5E, Supp Fig.S6C). Overall, we identified that 1) the anti-apoptotic protein BCL2A1 is a BCR-dependent resistance factor to Bcl2 inhibition; 2) BCL2A1 is selectively down-regulated through BTK inhibition, leading to ibrutinib/venetoclax synergistic apoptosis.

CARD11 **GOF mutations result in BCR-independent** ***BCL2A1*** **overexpression**

The CARD11-BCL10-MALT1 (CBM) complex is involved in the transduction of BCR-specific NFκB signaling by triggering MALT1 scaffold and protease activities (Fig.6A)[33]. We first observed constitutive CBM activity, through the cleavage of the MALT1 substrate HOIL1, in BCL2A1^{high} MCL cells but not in BCL2A1^{low} MCL cells (Supp Fig.S7A). This suggested that GOF mutations of *CARD11*, which are enriched in relapsed OAsIs patients, could have a direct impact on BCL2A1 expression. To test this hypothesis, we overexpressed *CARD11*^{WT}, *CARD11*^{G123S}, and *CARD11*^{G123D} in HEK293 cells, which lack CARD11 but express both BCL10 and MALT1. Both mutations resulted in increased activity of the CBM, measured by the cleavage of HOIL1 and CYLD (Supp Fig.7B). Using reporter assay experiments, we showed that *CARD11* GOF mutations led directly to increased activity of NFκB (fold change in *CARD11*^{MUT}= 4.2, p<0.001) as well as *BCL2A1* promoter activity (fold change in *CARD11*^{MUT}= 2.7, p<0.001, Fig.6B). These results suggest that GOF mutations in the latch domain of CARD11 lead directly to BCR-independent induction of NFκB/*BCL2A1*. Similar findings were obtained with GOF mutations in the CC domain (fold change in *CARD11*^{MUT}= 1.7, p<0.05; Supp Fig.S7C). Accordingly, ibrutinib greatly reduced *BCL2A1* level in

CARD11^{WT} (fold change = 0.21, n=4) but not in *CARD11*^{MUT} (fold change = 1.12, n=4) lymphoma cells (Fig.6C).

MALT1 targeting results in BCL2A1 inhibition and consequent synergistic cell death with BCL2 targeting, irrespective of CARD11 mutational status.

MALT1, in contrast to *CARD11* and *BCL10*, is significantly up-regulated in MCL cells when compared to normal B-cells (NBC) (Supp Fig.S7D), and selective inhibitors against its protease activity are currently being tested in early-phase trials. To address the potential efficacy of MALT1 inhibition for counteracting both BCR-dependent (*CARD11*^{WT}) and independent (*CARD11*^{MUT}) *BCL2A1* expression, we tested two highly selective MALT1 allosteric inhibitors, MLT-748[34] and JNJ-67856633[35]. Using reporter assay experiments, we first observed that MALT1 inhibition resulted in the inhibition of *CARD11*^{MUT}-dependent NFκB activity (Fold change = 0.59 for G123S, 0.56 for D230N, $p<0.05$, Supp Fig.S7C). Likewise, we observed that both inhibitors partially counteracted *CARD11*^{G123S}-dependent *BCL2A1* promoter activity (Fold inhibition MALT1-i vs. untreated= 0.59 for G123S, Supp Fig. S7E). Based on these encouraging results, we further performed RNA-seq of CARD11^{WT} and CARD11^{MUT} lymphoma cells treated with the BTK inhibitor ibrutinib or the MALT1 inhibitor MLT-748. BTK targeting resulted in the inhibition of genes belonging to the MCL_R16 signature, including *BCL2A1*, in *CARD11*^{WT} but not in *CARD11*^{MUT} cells ($p<0.0001$, Fig.7A left panel). By contrast, MALT1 inhibition similarly lowered gene expression in both groups including *BCL2A1,* which was down-regulated irrespective of *CARD11* status (Fig.7A right panel). This was further confirmed by q-PCR in *CARD11*^{WT} (fold change = 0.54, n=3) and *CARD11*^{MUT} cells (fold change = 0.51, n=3) and similar results were obtained using MLT-748 and JNJ-67856633 (Supp Fig.S8A-B).

MALT1 targeting resulted partial BCL2A1 protein down-regulation in all samples, including *CARD11*^{G123S} MCL cells, in contrast to BTK targeting whose efficacy was restricted to *CARD11*^{wt} cells (Fig.7B-C). Supporting the role of BCL2A1 in venetoclax resistance, we observed synergistic apoptosis after a MALT1/BCL2 targeted combination *in vitro* in both

BCL2A1+ *CARD11*^{WT} and *BCL2A1*+ *CARD11*^{MUT} (synergy score>10) (Fig.7D). As expected, synergy was not observed in *BCL2A1*- Z138 cells (synergy score: -4.7) (Supp Fig.S8C).

To address MALT1/BCL2 dual targeting in *CARD11*^{MUT} MCL cells *in vivo*, we used the chick embryo chorioallantoic membrane (CAM). This vascularized and immunodeficient alternative *in vivo* model allows the growth of numerous cell types[36]. Here, we established a CAM model using BTK-resistant[37] *CARD11*^{D230N} BCL2A1^{+} PDX cells, which were treated with the clinically available MALT1 inhibitor JNJ-67856633 alone or in combination with the BCL2 inhibitor venetoclax (Fig.7E, Supp Fig.S9A-C). While low doses of venetoclax showed no significant inhibition of tumor growth, JNJ-67856633 reduced tumor growth to 40 % of control. The combination highlighted a strong synergy leading to 70 % of tumor growth inhibition after 4 days of treatment (Fig.7E). These results were confirmed in NSG mice, the *CARD11*^{D230N} BCL2A1^{+} tumor burden (PB and spleen) being reduced using a combination of JNJ-67856633 and venetoclax, both in sub-optimal concentrations as a single agent (Supp Fig.S9D-F).

Discussion

Based on single-cell resolution analysis of longitudinal samples from a patient enrolled on the OAsIs trial, we identified, at baseline, a minor cellular population that persisted upon treatment *in vivo* and ultimately gave rise to relapse. The transcriptomic signature of this minor population was enriched in genes that are controlled by *NFKB1*, highlighting the fact that a BTK-independent NFkB program was involved in the resistance to the OAsIs regimen *in vivo*. The resistance signature was the basis for a 16-gene score, which also retrospectively predicted lower OS/PFS in patients treated with chemotherapy. Overall, our results suggested overlapping resistance mechanisms for both chemotherapy and targeted therapies in MCL. A subset of multi-resistant MCL patients, whose disease progressed on chemotherapy, BTK/BCL2-based targeted therapy, and CAR-T cells, is emerging, however little is known about the (poly)resistance mechanisms involved[38]. It would now be interesting to examine whether tumoral cells from these very high-risk MCL patients display a similar NFkB1-related resistance profile and whether alternative strategies, such as bi-specific antibodies[39,40], can counteract this resistance.

BTK-independent NFkB activation can be initiated in malignant B-cells by using multiple pathways which have been implicated in BTK inhibition resistance[16,41]. This signaling is triggered by genetic events[15,26], epigenetic regulation[42] and microenvironmental cues[13,20]. In the present study, we have observed that *CARD11* GOF mutations were enriched at OAsIs relapse and resulted in increased NFkB activity. *CARD11* GOF mutations are observed in nearly 10% of NHL at diagnosis[43], and allow cell survival upon BTK inhibition by restoring NFkB signaling downstream. Accordingly, *CARD11* GOF mutations have been associated with *in vivo* ibrutinib resistance in DLBCL[25] and FL[44]. We have demonstrated here that a similar pattern is found in MCL. Intriguingly, we have observed enrichment of *CARD11* mutations within the latch domain (Supp Table S4). This pattern was confirmed in a recent analysis of recurrently mutated genes in several B-cell NHL subtypes at diagnosis, in which CARD11 mutants were enriched in the G123 (3/11) and D230 (3/11) positions in MCL, but

not in FL, DLBCL, or BL[43]. In the present study, we have demonstrated that both variants induced elevated NFkB activity *in vitro,* and a recent multiplex functional assessment of genetic variants ranked the G123S as one of the most efficient in escaping ibrutinib treatment[45]. In addition, elevated NFkB activation associated with *CARD11* germline mutation at the G123 position has been described in the context of BENTA disease[21], reinforcing the potent GOF associated with this hotspot.

By integrating multi-omics and functional analysis, we have demonstrated here that GOF mutations result in NFkB-dependent induction of BCL2A1. Recent publications have highlighted its critical role in venetoclax resistance in hematological malignancies[12,29,46]. Our BH3-profiling results suggest the dynamic sequestration of the BH3-only proteins by BCL2A1 at the mitochondrial level after targeting BCL2, MCL1, and BCLXL, as recently described in CLL[30]. Accordingly, overexpression of BCL2A1 led to increased resistance to the OAsIs combination, highlighting the need to target this anti-apoptotic protein to counteract resistance. No selective small molecule has yet been developed to specifically target BCL2A1 but we have demonstrated here that BCL2A1 is tightly controlled by the BTK/BCR pathway in CARD11^{wt} MCL. Altogether, our results position BCL2A1 as a selective bridge between the BCR pathway and mitochondrial apoptosis. Accordingly, BCL2A1 expression is greatly inhibited by ibrutinib in CARD11^{wt} cells, but not in CARD11^{MUT} cells, which results in ibrutinib/venetoclax synergy in CARD11^{wt} BCL2A1^{+} lymphoma cells exclusively.

CARD11 forms the CBM complex with MALT1, which has emerged as an attractive therapeutic target, several molecules that target its protease function being tested in vitro and *in vivo*[47-49]. Moreover, recent studies have demonstrated that MCL cells are addicted to MALT1, at least partially inherited from their B1a B-cell origin[50,51]. We have demonstrated that inhibition of the MALT1 protease function resulted in the inhibition of the MCL_R16 signature, including *BCL2A1*, and synergized with BCL2 inhibition to induce apoptosis, irrespective of the CARD11 mutational status. Overall, our results have highlighted that

MALT1 targeting could be an interesting alternative to BTK inhibitors, especially in the context of CARD11^{MUT} cells, although MALT1 inhibitors lead to a less profound inhibition of BCL2A1 compared to BTK inhibition in CARD11^{WT} cells. Several strategies for inhibiting both MALT1 scaffold and protease functions, such as the PROTAC technology that leads to selective protein degradation[52], are under pre-clinical evaluation and may lead to increased efficacy of MALT1 targeting in the near future.

To summarize, our data have uncovered the control of mitochondrial apoptosis by CARD11 through BCL2A1 expression. This network is crucially involved in the resistance to BTK/BCL2-based targeted inhibition, as CARD11 GOF mutations lead not only to BCR independence and consequently ibrutinib resistance, but also to BCL2A1-mediated venetoclax resistance. Nevertheless, our data has shown that targeting the CBM through MALT1 inhibition reverts this resistance and that MALT1 targeting appears to be a promising therapeutic option for counteracting resistance, especially in the context of CARD11 mutation. Mutations in CARD11 are frequently found in DLBCL, for which there is a growing interest in BTK/BCL2-based targeted therapy[53]. Our results, which describe the role of the CARD11-NFkB-BCL2A1 axis in MCL resistance *in vivo,* could be applied to a broad spectrum of hematological malignancies.

Contribution

SD designed and performed the experiments and analyzed data. CB performed the experiments and bioinformatics analysis and analyzed data. YLB, CM, DB, CD, AM, ED, and AMA performed experiments and analyzed data. JJ and NB performed NFκB and BCL2A1 Luciferase Assay and analyzed data. JCS and GR performed experiments on CAM model and analyzed data. CK performed experiments on NSG mice and analyzed data. PM, SM, BT and SLG participated in the design of the study. CPD participated in the design of the study, in the data analysis, and in writing the article. DC designed the study, analyzed data, and wrote the article.

Acknowledgments

The authors would like to thank the patients who agreed to be part of the Refract-Lyma cohort. The authors thank la Ligue Contre le Cancer Grand-Ouest, i-Site NexT (ANR-16-IDEX-0007), the SIRIC ILIAD (INCa-DGOS-Inserm-ITMO Cancer_12558 and INCa-DGOS-Inserm-ITMO Cancer_18011) and Action Cancer 44. The authors thank Drs. Gangoda L. and Herold MJ. for kindly providing the Bfl1-specific monoclonal antibody and Dr. Andrew L. Snow for kindly providing the pUNO1-hCARD11 plasmids. The authors thank Magali Devic for expert technical assistance. We are most grateful to the Genomics Core Facility GenoA, member of Biogenouest and France Genomique and to the Bioinformatics Core Facility BiRD, member of Biogenouest and Institut Français de Bioinformatique (IFB) (ANR-11-INBS-0013) for the use of their resources and their technical support. The authors acknowledge the Cytocell-Flow Cytometry and FACS core facility (SFR Bonamy, BioCore, Inserm UMS 016, CNRS UAR 3556, Nantes, France) for its technical expertise and help, member of the Scientific Interest Group (GIS) Biogenouest and the Labex IGO program supported by the French National Research Agency (n°ANR-11-LABX-0016-01).

Fig. Legends

Fig. 1. Comprehensive genomic analysis of MCL patients enrolled in the OAsIs trial

(A) Schematic representation of the experimental design to identify therapeutic resistance in MCL. MCL patients were included in the OAsIs clinical trial (obinutuzumab (Anti-CD20), ibrutinib (BTK-i) and venetoclax (BCL2-i)). Blood or bone marrow samples were collected at inclusion or relapse and targeted DNA-seq of 49 selected genes plus the 9p21 region was performed.

(B-D) Landscape of recurrent mutations (SNV/indel) and copy number variations (amplification/deletion) in the patients enrolled in OAsIs and detected by deep DNA-seq at inclusion (incl., n=12) **(B)**, relapse (Rel., n=5) **(C)** or in longitudinal samples **(D)**. Each column represents an individual sample/patient. Only genes with at least two anomalies detected in the cohort and with a variant frequency greater than 5% are represented. Statistical significance was determined by a two-tailed Fisher's exact test. CR: complete response, PR: partial response, PD: progression disease.

(E) The fish plot shows the clonal evolution pattern of patient 34 based on the variant frequency (VaF) measured at diagnosis (Diag), inclusion (incl.), and relapse (Rel.) (Supp Table S2) and normalized to the $TP53^{Y220C}$ VaF. SD: Stable Disease.

(F) Schematic representation of CARD11 domains and the mutations found in our Refract-Lyma cohort (n=62 sequenced for CARD11), including patients enrolled in OAsIs trial.

Fig. 2. Longitudinal single-cell RNA-seq analysis of MCL during OAsIs

(A) UMAP plots of the cells from patient MCL34 at inclusion (incl.) and at relapse (Rel) after OAsIs treatment. Each dot represents a single cell. UMAP plots display the NIK/ NFκB2 (left panel), NFκB1 (middle panel) and BCR (right panel) signature scores at inclusion and relapse. Wilcoxon sign-rank test. **** p adj < 0.0001

(B) UMAP plot of the 7 clusters identified by Seurat at inclusion (incl.) and at relapse (Rel) after OAsIs treatment for the patient MCL34. The cell proportion for each cluster at inclusion (green) or relapse (pink) is indicated at the bottom.

(C) UMAP plot displaying the cell-cycle signature scores at inclusion and relapse for the patient MCL34. Cell proportion of cycling (red) or resting (grey) in each cluster is indicated at the bottom.

(D) Trajectory of single cells at inclusion (incl.) and at relapse (Rel) using Monocle2. Clusters defined in panel B are identified in the lower panel.

(E) Heatmap showing the top 20 genes for each cluster. The color gradient indicates the intensity of the median gene expression as indicated. Functional enrichment pathway was calculated using Reactome and Enrichr. **** p adj < 0.0001.

Fig. 3. **OAsIs resistance score predicts a less favorable outcome in MCL.**

(A) The sign_clust5 score was computed based on the 742 genes characteristic of cluster #5 of patient MCL34, as represented in Fig. 2E. The violin plot shows the sign_clust5 score for patients who achieved complete response (MCL36, MCL39), rapid relapse after the initial response (MCL34, MCL12), or progression (MCL10, MCL24). The analysis was performed at the whole sample level (upper panel) or at Seurat computed cluster level (lower panel). Mann-Whitney test. ***p<.001, ****p<.0001.

(B) Sixteen genes comprising a novel OAsIs resistance score (MCL_R16) based on the top genes of the sign_clust5 signature.

(C) The MCL_R16 score was computed at Seurat-computed cluster level in MCL34 and MCL12 at the time of inclusion. Mann-Whitney test. ****p<.0001.

(D) Kaplan–Meier analyses of overall survival or progression-free survival (PFS) for the MCL_R16, cell-cycle, BCR, and NFκB signatures. Probabilities were calculated on 122 MCL patients treated with R-CHOP (GSE93291) or on 99 MCL patients included in the LYMA cohort (LYMA_RNA-seq) respectively. Black curve: low score, red curve: high score. Log-Rank test.

Fig. 4. **Identification of BCL2A1 as a resistance factor to OAsIs combination**

(A) scRNA-seq analysis of *BCL2A1* gene expression at inclusion (incl.) or relapse (Rel) in all OAsIs samples available (left panel) or longitudinal samples from patient MCL34. Each dot represents a cell. Wilcoxon-sign-rank test. ****p<.0001.

(B) Bulk RNA-seq analysis of *BCL2A1* gene expression in peripheral blood MCL cells (PB, n=63) or MCL cell lines (n=7).

(C) BCL2A1 protein expression in primary PB MCL cells (n=8), Maver, and NTS3 cell lines, and in OAsIs samples (MCL 24 and MCL36) was evaluated by immunoblot.

(D) Survival of Mino_ct and Mino_A1 (Supp Fig. S5) treated with single-agent Venetoclax at indicated doses or with OAsIs combination (Ibrutinib, 500 nM; Obinutuzumab 500 ng/ml) for 48h. Cell viability was measured by the lack of Annexin-V staining. ANOVA test. ****p<.0001. The mean and SD of three independent experiments are represented.

(E) BCL2A1 specific BH3-profiling was performed using the selective peptide FS2 (20 µM) in venetoclax-sensitive Mino cells (left panel) and venetoclax-resistant SP53 cells (right panel). Mino cells were pretreated or not with Venetoclax at indicated doses. SP53 cells were pretreated or not with Venetoclax (VNT, 500 nM), S63845 (S63, 500 nM) and A1155463 (A11, 500 nM) for 6h before cytochrome-C release measurement. ANOVA test. ***p<.001. The mean and SD of three independent experiments are represented.

Fig. 5. **BCR-dependent expression of BCL2A1 in MCL**

(A) Correlation between BCR signature and *BCL2A1* gene expression in peripheral blood (PB) MCL cells (n=63) and MCL cell lines (n=7). Spearman r and p-value are indicated on the graph.

(B) *BCL2A1* expression in PB MCL cells (n=3), and MCL cell lines (MAVER-1, UPN1) treated or not for 3h with anti-IgM (αIgM, 10 µg/ml) was measured by RT-qPCR.. paired t-test. *p<.05.

(C) BCL2A1 protein expression in MCL primary cells (n=6) and NTS3 cell line treated or not for 3h with anti-IgM (αIgM, 10 µg/ml) was assessed by immunoblot.

(D) *CD83, BCL2A1, BCL2, MCL1* and *BCLXL* gene expression in BCL2A1 positive MCL cell lines (SP53, NTS3, REC-1, Mino) treated for 24h with Ibrutinib (500 nM) was evaluated by bulk RNA-sequencing. ANOVA test. **p<.01, *p<.05

(E) Synergy score (HSA method) computed for 6 MCL cell lines treated with venetoclax and ibrutinib for 48h. Unpaired t-test. *p<.05. Detailed results are represented in Supp Fig.S6C. The mean and SD of three independent experiments are represented.

Fig. 6. **BCR-independent expression of BCL2A1 in CARD11 mutated cells.**

(A) B-cell receptor (BCR) signaling triggers the NFkB1 pathway through the activation of several proteins such as BTK, which can be inhibited by ibrutinib, and complexes such as CARD11/BCL10/MALT1 (CBM). Several previously described CBM substrates are mentioned including HOIL1, which is used in the following experiments as a marker of CBM activity.

(B) NFκB luciferase assay (left panel) and *BCL2A1* promoter LightSwitch™ luciferase assay (right panel) in HEK293 cells transfected with a pUNO1 (empty), pUNO1-hCARD11-WT, pUNO1-hCARD11-G123S or pUNO1-hCARD11-G123D vector (48h). 2way ANOVA. ****p<.0001, ***p<.001, **p<.01, *p<.05. The mean and SD of three independent experiments are represented.

(C) *BCL2A1* gene expression was measured by RT-qPCR in $CARD11^{WT}$ MCL (SP53, NTS3, and REC-1) and DLBCL (U2932) cell lines and $CARD11^{MUT}$ MCL cells (001-024, DFBL) and DLBCL (OCILY3, SUDHL16) cell lines treated with ibrutinib (500 nM) for 6h. Detailed CARD11 mutational status is described in Supp Table S4. Mann-Whitney test. *p < 0.05.

Fig. 7 Identification of MALT1 as a target to overcome OAsIs resistance

(A) RNA-seq expression of the 16 genes of the MCL_R16 resistance signature in BCL2A1^{+} CARD11^{WT} cell lines (SP53, NTS3, REC-1) and BCL2A1^{+} CARD11^{MUT} cells (001-024, OCILY3, SUDHL16) treated 24h with the BTK inhibitor Ibrutinib (500 nM) **(left panel)** or the MALT1 inhibitor MLT-748 (1 µM) **(right panel)**. Mann-Whitney test. ****p<.0001. n.s.: not significant. *BCL2A1* is shown in red. Genes from bottom to top: *CCL4, FABP5, CCL3, BCL2A1, CCL22, NPW, NME1, PTP4A3, PLEK, CD83, SRM, CALR, PA2G4, NCL, SDF2L1, DDX21*.

(B-C) CARD11, HOIL1, and BCL2A1 protein expression were assessed by immunoblot in indicated cells treated or not with the BTK inhibitor ibrutinib (500 nM) or the MALT1 inhibitor MLT-748 (1 µM) for 24h. The arrow highlights cleaved form of HOIL1.

(D) Synergy score (HSA method) computed for 4 cell lines treated with venetoclax and MLT-748 for 48h. Unpaired t-test. *p<.05. Detailed results are represented in Supp Fig. S8C. The mean and SD of three independent experiments are represented.

(E) Tumor weights at day 16 for CARD11^{D230N} MCL PDX (DFBL44685-v2) treated with the BCL2-i venetoclax (2 nM), the MALT1-i JNJ-67856633 (250-500 nM) or both. n = 5 per group. Mann-Whitney test. **p<.01. n.s.: not significant. Representative pictures of engrafted tumors in CAM at day 16 are shown in the right panel.

Disclosures

No potential conflicts of interest were disclosed by the other authors.

References

1. Saleh K, Cheminant M, Chiron D, Burroni B, Ribrag V, Sarkozy C. Tumor Microenvironment and Immunotherapy-Based Approaches in Mantle Cell Lymphoma. *Cancers*. 2022;14(13):3229.
2. Yi S, Yan Y, Jin M, et al. Genomic and transcriptomic profiling reveals distinct molecular subsets associated with outcomes in mantle cell lymphoma. *The Journal of Clinical Investigation*. 2022;132(3).
3. Prevodnik VK, Lavrenčak J, Horvat M, Novakovič BJ. The predictive significance of CD20 expression in B-cell lymphomas. *Diagnostic pathology*. 2011;6(1):1-6.
4. Tessoulin B, Papin A, Gomez-Bougie P, et al. BCL2-family dysregulation in B-cell malignancies: from gene expression regulation to a targeted therapy biomarker. *Frontiers in oncology*. 2019;8:645.
5. Chang BY, Francesco M, De Rooij MF, et al. Egress of CD19+ CD5+ cells into peripheral blood following treatment with the Bruton tyrosine kinase inhibitor ibrutinib in mantle cell lymphoma patients. *Blood, The Journal of the American Society of Hematology*. 2013;122(14):2412-2424.
6. Davids MS, Roberts AW, Seymour JF, et al. Phase I first-in-human study of venetoclax in patients with relapsed or refractory non-Hodgkin lymphoma. *Journal of Clinical Oncology*. 2017;35(8):826.
7. Wang ML, Rule S, Martin P, et al. Targeting BTK with ibrutinib in relapsed or refractory mantle-cell lymphoma. *New England Journal of Medicine*. 2013;369(6):507-516.
8. Le Gouill S, Thieblemont C, Oberic L, et al. Rituximab after autologous stem-cell transplantation in mantle-cell lymphoma. *New England Journal of Medicine*. 2017;377(13):1250-1260.
9. Wang ML, Jurczak W, Jerkeman M, et al. Ibrutinib plus bendamustine and rituximab in untreated mantle-cell lymphoma. *New England Journal of Medicine*. 2022;386(26):2482-2494.
10. Eyre TA, Walter HS, Iyengar S, et al. Efficacy of venetoclax monotherapy in patients with relapsed, refractory mantle cell lymphoma after Bruton tyrosine kinase inhibitor therapy. *Haematologica*. 2019;104(2):e68.
11. Martin P, Maddocks K, Leonard JP, et al. Postibrutinib outcomes in patients with mantle cell lymphoma. *Blood, The Journal of the American Society of Hematology*. 2016;127(12):1559-1563.
12. Zhao X, Ren Y, Lawlor M, et al. BCL2 amplicon loss and transcriptional remodeling drives ABT-199 resistance in B cell lymphoma models. *Cancer Cell*. 2019;35(5):752-766. e759.
13. Chiron D, Bellanger C, Papin A, et al. Rational targeted therapies to overcome microenvironment-dependent expansion of mantle cell lymphoma. *Blood, The Journal of the American Society of Hematology*. 2016;128(24):2808-2818.
14. Thus YJ, Eldering E, Kater AP, Spaargaren M. Tipping the balance: toward rational combination therapies to overcome venetoclax resistance in mantle cell lymphoma. *Leukemia*. 2022:1-12.
15. Chiron D, Di Liberto M, Martin P, et al. Cell-Cycle Reprogramming for PI3K Inhibition Overrides a Relapse-Specific C481S BTK Mutation Revealed by Longitudinal Functional Genomics in Mantle Cell LymphomaOverriding Relapse-Specific BTK Mutation in MCL. *Cancer discovery*. 2014;4(9):1022-1035.
16. Ondrisova L, Mraz M. Genetic and non-genetic mechanisms of resistance to BCR signaling inhibitors in B cell malignancies. *Frontiers in oncology*. 2020;10:591577.
17. Zhang L, Yao Y, Zhang S, et al. Metabolic reprogramming toward oxidative phosphorylation identifies a therapeutic target for mantle cell lymphoma. *Science translational medicine*. 2019;11(491):eaau1167.
18. Chiron D, Dousset C, Brosseau C, et al. Biological rational for sequential targeting of Bruton tyrosine kinase and Bcl-2 to overcome CD40-induced ABT-199 resistance in mantle cell lymphoma. *Oncotarget*. 2015;6(11):8750.
19. Le Gouill S, Morschhauser F, Chiron D, et al. Ibrutinib, obinutuzumab, and venetoclax in relapsed and untreated patients with mantle cell lymphoma: a phase 1/2 trial. *Blood*. 2021;137(7):877-887.
20. Decombis S, Papin A, Bellanger C, et al. The IL32/BAFF axis supports prosurvival dialogs in the lymphoma ecosystem and is disrupted by NIK inhibition. *Haematologica*. 2022.

21. Brohl AS, Stinson JR, Su HC, et al. Germline CARD11 mutation in a patient with severe congenital B cell lymphocytosis. *Journal of clinical immunology*. 2015;35(1):32-46.
22. Snow AL, Xiao W, Stinson JR, et al. Congenital B cell lymphocytosis explained by novel germline CARD11 mutations. *Journal of Experimental Medicine*. 2012;209(12):2247-2261.
23. Takeuchi M, Rothe M, Goeddel DV. Anatomy of TRAF2: distinct domains for nuclear factor-κB activation and association with tumor necrosis factor signaling proteins. *Journal of Biological Chemistry*. 1996;271(33):19935-19942.
24. Lenz G, Davis RE, Ngo VN, et al. Oncogenic CARD11 mutations in human diffuse large B cell lymphoma. *Science*. 2008;319(5870):1676-1679.
25. Caeser R, Walker I, Gao J, et al. Acquired CARD11 mutation promotes BCR independence in Diffuse Large B Cell Lymphoma. *JCO precision oncology*. 2021;5.
26. Rahal R, Frick M, Romero R, et al. Pharmacological and genomic profiling identifies NF-κB–targeted treatment strategies for mantle cell lymphoma. *Nature medicine*. 2014;20(1):87-92.
27. Saba NS, Liu D, Herman SE, et al. Pathogenic role of B-cell receptor signaling and canonical NF-κB activation in mantle cell lymphoma. *Blood, The Journal of the American Society of Hematology*. 2016;128(1):82-92.
28. Rauert-Wunderlich H, Rudelius M, Berberich I, Rosenwald A. CD40L mediated alternative NFκB-signaling induces resistance to BCR-inhibitors in patients with mantle cell lymphoma. *Cell death & disease*. 2018;9(2):1-9.
29. Esteve-Arenys A, Garcia-Valero J, Gonzalez D, et al. Pharmacological downregulation of BFL-1 by the BET bromodomain inhibitor CPI203 overcomes ABT-199 resistance in MYC+/BCL2+ double hit lymphoma. *Cancer Research*. 2017;77(13_Supplement):2161-2161.
30. Haselager MV, Kielbassa K, Ter Burg J, et al. Changes in Bcl-2 members after ibrutinib or venetoclax uncover functional hierarchy in determining resistance to venetoclax in CLL. *Blood*. 2020;136(25):2918-2926.
31. Jenson JM, Ryan JA, Grant RA, Letai A, Keating AE. Epistatic mutations in PUMA BH3 drive an alternate binding mode to potently and selectively inhibit anti-apoptotic Bfl-1. *Elife*. 2017;6:e25541.
32. Prazma CM, Yazawa N, Fujimoto Y, Fujimoto M, Tedder TF. CD83 expression is a sensitive marker of activation required for B cell and CD4+ T cell longevity in vivo. *The Journal of Immunology*. 2007;179(7):4550-4562.
33. Seshadri MR, Melnick AM. Targeting MALT1 for the treatment of diffuse large B-cell lymphoma. *Leukemia & Lymphoma*. 2022;63(4):789-798.
34. Quancard J, Klein T, Fung S-Y, et al. An allosteric MALT1 inhibitor is a molecular corrector rescuing function in an immunodeficient patient. *Nature chemical biology*. 2019;15(3):304-313.
35. Philippar U, Lu T, Vloemans N, et al. Discovery of JNJ-67856633: A novel, first-in-class MALT1 protease inhibitor for the treatment of B cell lymphomas. *Cancer Research*. 2020;80(16_Supplement):5690-5690.
36. Miebach L, Berner J, Bekeschus S. In ovo model in cancer research and tumor immunology. *Frontiers in Immunology*. 2022:5793.
37. Dobrovolsky D, Wang ES, Morrow S, et al. Bruton tyrosine kinase degradation as a therapeutic strategy for cancer. *Blood, The Journal of the American Society of Hematology*. 2019;133(9):952-961.
38. Jain P, Wang ML. Mantle cell lymphoma in 2022—A comprehensive update on molecular pathogenesis, risk stratification, clinical approach, and current and novel treatments. *American journal of hematology*. 2022;97(5):638-656.
39. Phillips T, Dickinson M, Morschhauser F, et al. Glofitamab Step-up Dosing Induces High Response Rates in Patients (pts) with Relapsed or Refractory (R/R) Mantle Cell Lymphoma (MCL), Most of Whom Had Failed Prior Bruton's Tyrosine Kinase Inhibitor (BTKi) Therapy. *Blood*. 2021;138:130.
40. van der Horst HJ, de Jonge AV, Hiemstra IH, et al. Epcoritamab induces potent anti-tumor activity against malignant B-cells from patients with DLBCL, FL and MCL, irrespective of prior CD20 monoclonal antibody treatment. *Blood cancer journal*. 2021;11(2):1-8.
41. Balaji S, Ahmed M, Lorence E, Yan F, Nomie K, Wang M. NF-κB signaling and its relevance to the treatment of mantle cell lymphoma. *Journal of hematology & oncology*. 2018;11(1):1-11.

42. Shaffer AL, Phelan JD, Wang JQ, et al. Overcoming Acquired Epigenetic Resistance to BTK Inhibitors Overcoming Acquired Epigenetic Resistance to BTK Inhibitors. *Blood cancer discovery*. 2021;2(6):630-647.
43. Ma MCJ, Tadros S, Bouska A, et al. Subtype-specific and co-occurring genetic alterations in B-cell non-Hodgkin lymphoma. *Haematologica*. 2022;107(3):690.
44. Bartlett NL, Costello BA, LaPlant BR, et al. Single-agent ibrutinib in relapsed or refractory follicular lymphoma: a phase 2 consortium trial. *Blood, The Journal of the American Society of Hematology*. 2018;131(2):182-190.
45. Meitlis I, Allenspach EJ, Bauman BM, et al. Multiplexed functional assessment of genetic variants in CARD11. *The American Journal of Human Genetics*. 2020;107(6):1029-1043.
46. Zhang H, Nakauchi Y, Köhnke T, et al. Integrated analysis of patient samples identifies biomarkers for venetoclax efficacy and combination strategies in acute myeloid leukemia. *Nature cancer*. 2020;1(8):826-839.
47. Jiang VC, Liu Y, Lian J, et al. Cotargeting of BTK and MALT1 overcomes resistance to BTK inhibitors in mantle cell lymphoma. *The Journal of Clinical Investigation*. 2023;133(3).
48. Minderman M, Lantermans HC, Grüneberg LJ, et al. MALT1-dependent cleavage of CYLD promotes NF-κB signaling and growth of aggressive B-cell receptor-dependent lymphomas. *Blood cancer journal*. 2023;13(1):37.
49. Shah SB, Carlson CR, Lai K, et al. Combinatorial treatment rescues tumour-microenvironment-mediated attenuation of MALT1 inhibitors in B-cell lymphomas. *Nature Materials*. 2023:1-13.
50. Dai B, Grau M, Juilland M, et al. B-cell receptor–driven MALT1 activity regulates MYC signaling in mantle cell lymphoma. *Blood, The Journal of the American Society of Hematology*. 2017;129(3):333-346.
51. Pieters T, T'Sas S, Vanhee S, et al. Cyclin D2 overexpression drives B1a-derived MCL-like lymphoma in mice. *Journal of Experimental Medicine*. 2021;218(10):e20202280.
52. Fontan L, Hatcher J, Scott D, et al. Chemically Induced Degradation of MALT1 to Treat B-Cell Lymphomas. *Blood*. 2019;134:2073.
53. Bertram K, Leary PJ, Boudesco C, et al. Inhibitors of Bcl-2 and Bruton's tyrosine kinase synergize to abrogate diffuse large B-cell lymphoma growth in vitro and in orthotopic xenotransplantation models. *Leukemia*. 2022;36(4):1035-1047.

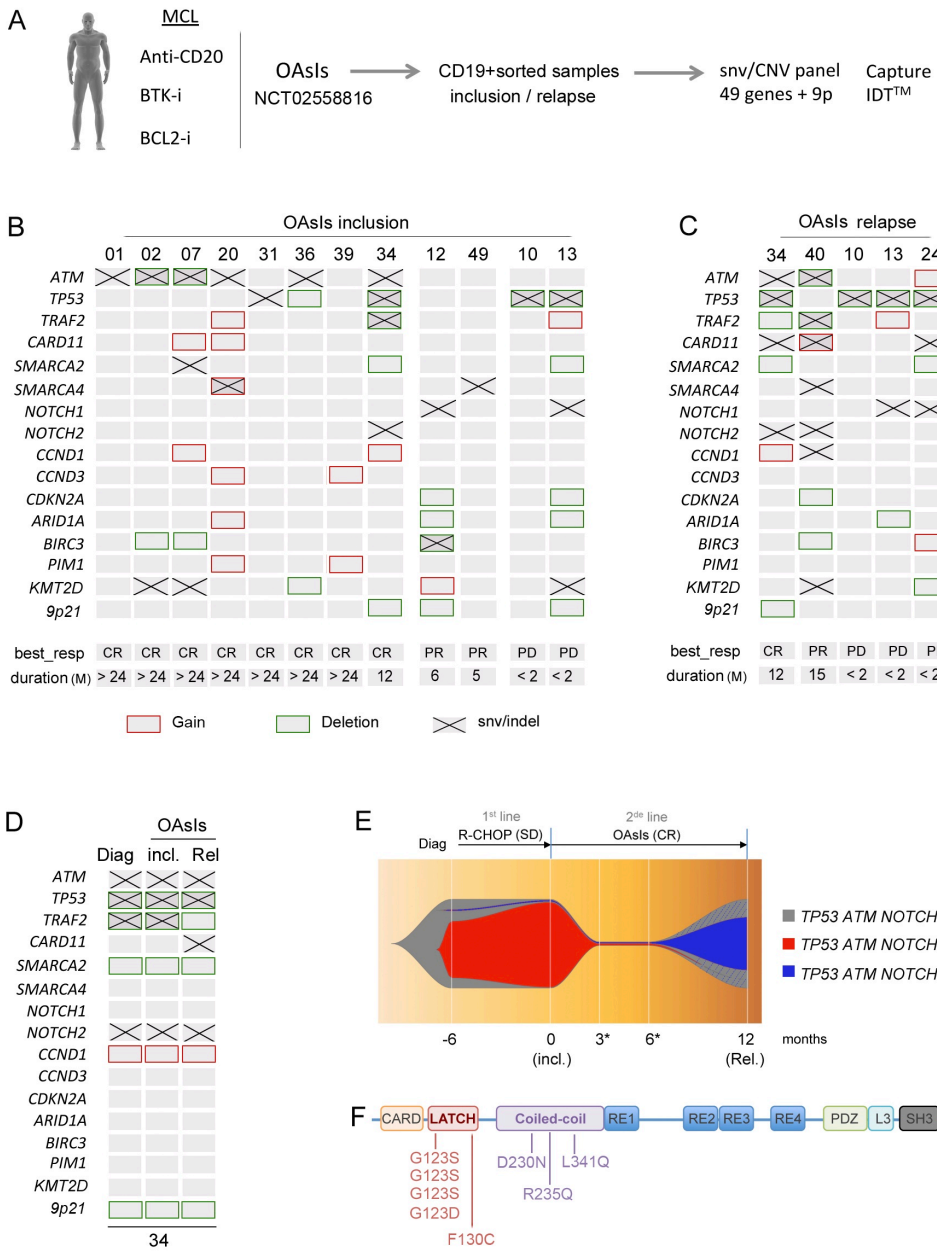
A
MCL
Anti-CD20
BTK-i
BCL2-i
OAsIs
NCT02558816
CD19+sorted samples
inclusion / relapse
snv/CNV panel
49 genes + 9p
Capture
IDT™
B
OAsIs inclusion
01 02 07 20 31 36 39 34 12 49 10 13
ATM
TP53
TRAF2
CARD11
SMARCA2
SMARCA4
NOTCH1
NOTCH2
CCND1
CCND3
CDKN2A
ARID1A
BIRC3
PIM1
KMT2D
9p21
best_resp CR CR CR CR CR CR CR CR PR PR PD PD
duration (M) > 24 > 24 > 24 > 24 > 24 > 24 > 24 12 6 5 < 2 < 2
Gain
Deletion
snv/indel
C
OAsIs relapse
34 40 10 13 24
ATM
TP53
TRAF2
CARD11
SMARCA2
SMARCA4
NOTCH1
NOTCH2
CCND1
CCND3
CDKN2A
ARID1A
BIRC3
PIM1
KMT2D
9p21
best_resp CR PR PD PD PD
duration (M) 12 15 < 2 < 2 < 2
D
OAsIs
Diag incl. Rel
ATM
TP53
TRAF2
CARD11
SMARCA2
SMARCA4
NOTCH1
NOTCH2
CCND1
CCND3
CDKN2A
ARID1A
BIRC3
PIM1
KMT2D
9p21
34
E
1st line
2de line
Diag
R-CHOP (SD)
OAsIs (CR)
TP53 ATM NOTCH2
TP53 ATM NOTCH2 TRAF2 C49F
TP53 ATM NOTCH2 CARD11 G123S
-6
0
(incl.)
3*
6*
12
(Rel.)
months
F
CARD
LATCH
Coiled-coil
RE1
RE2
RE3
RE4
PDZ
L3
SH3
L4
GUK
G123S
G123S
G123S
G123D
F130C
D230N
R235Q
L341Q

Figure 1

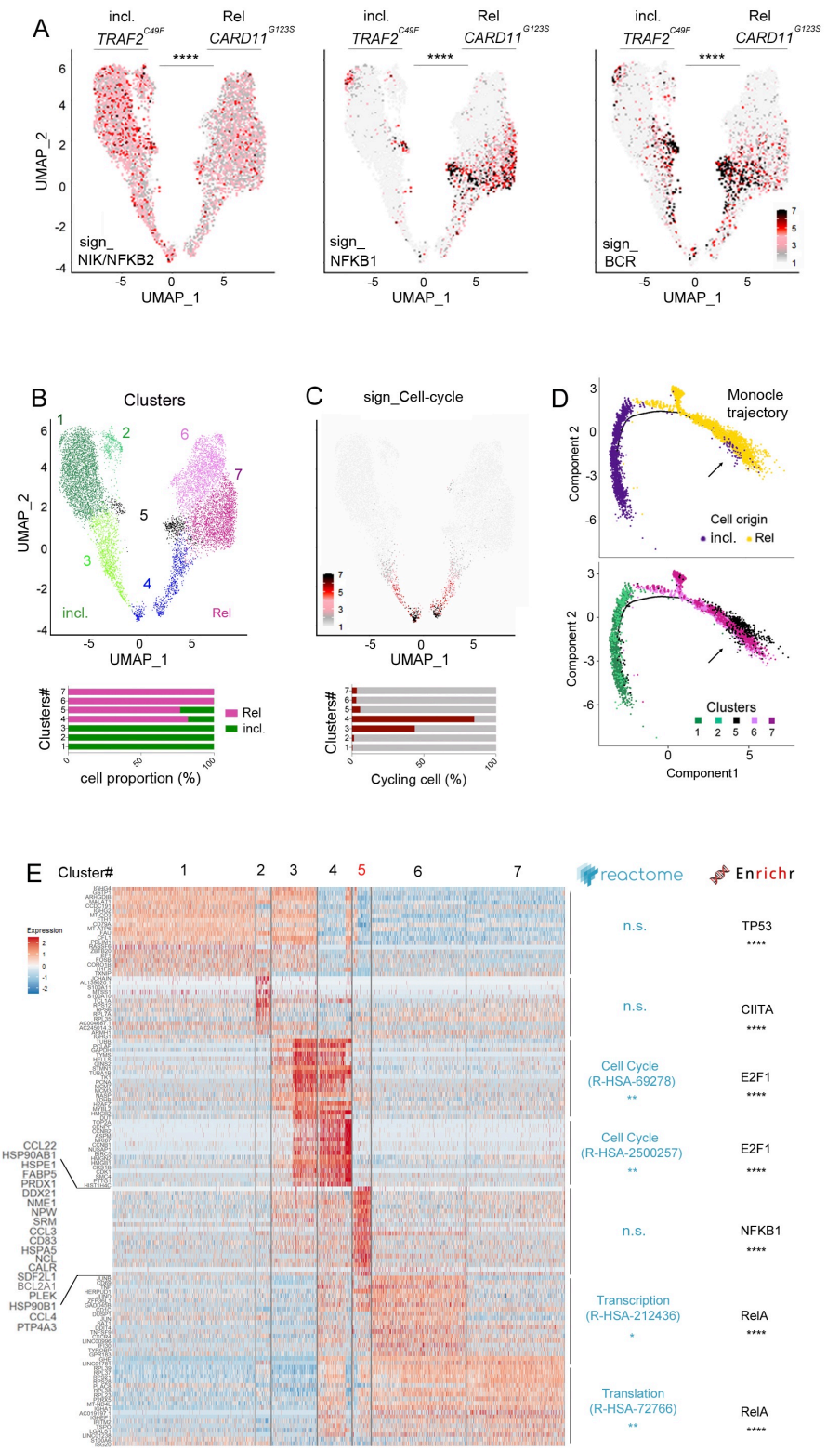
A
incl. TRAF2C49F
Rel CARD11G123S
****
sign_ NIK/NFKB2
sign_ NFKB1
sign_ BCR
UMAP_1
UMAP_2
B
Clusters
incl.
Rel
Clusters#
cell proportion (%)
C
sign_Cell-cycle
Cycling cell (%)
D
Monocle trajectory
Cell origin
Component 1
Component 2
E
Cluster#
Expression
CCL22
HSP90AB1
HSPE1
FABP5
PRDX1
DDX21
NME1
NPW
SRM
CCL3
CD83
HSPA5
NGI
CALR
SDF2L1
BCL2A1
PLEK
HSP90B1
CCL4
PTP4A3
reactome
Enrichr
n.s.
TP53
CIITA
Cell Cycle (R-HSA-69278)
E2F1
Cell Cycle (R-HSA-2500257)
NFKB1
Transcription (R-HSA-212436)
RelA
Translation (R-HSA-72766)

Figure 2

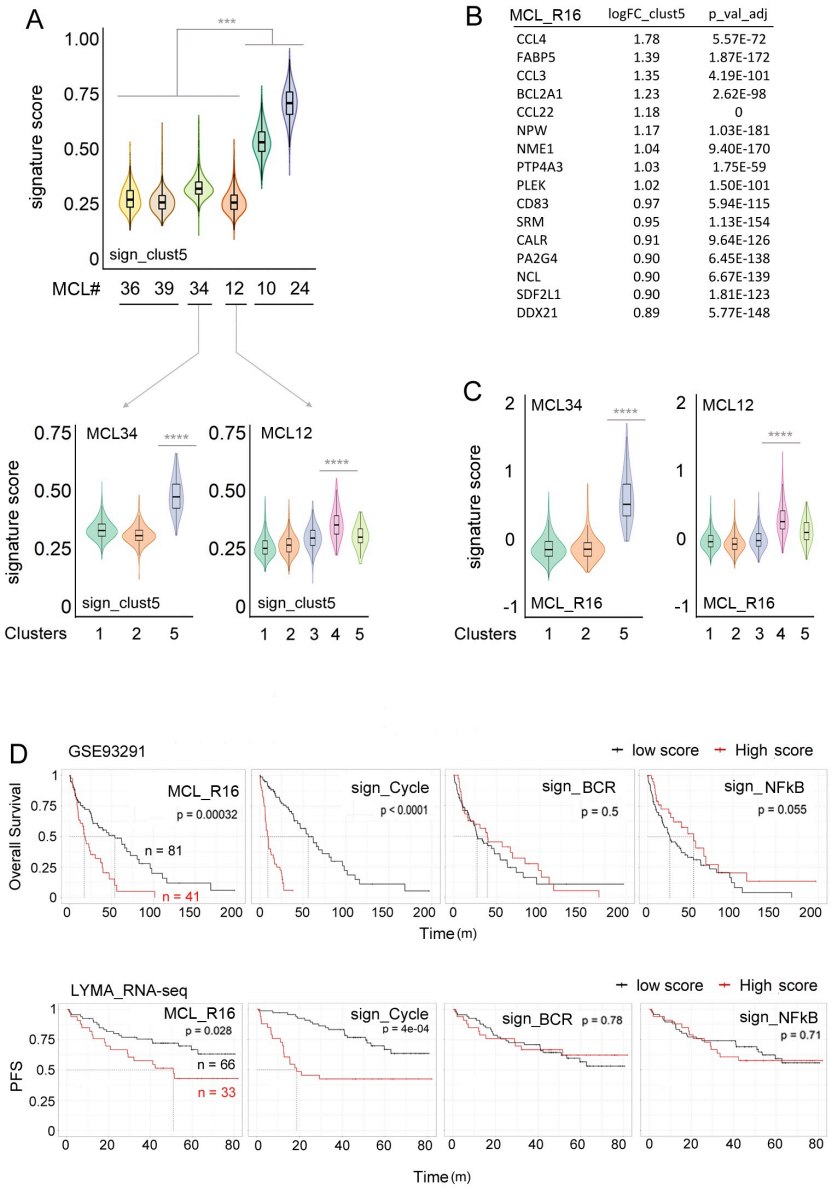

MCL_R16	logFC_clust5	p_val_adj
CCL4	1.78	5.57E-72
FABP5	1.39	1.87E-172
CCL3	1.35	4.19E-101
BCL2A1	1.23	2.62E-98
CCL22	1.18	0
NPW	1.17	1.03E-181
NME1	1.04	9.40E-170
PTP4A3	1.03	1.75E-59
PLEK	1.02	1.50E-101
CD83	0.97	5.94E-115
SRM	0.95	1.13E-154
CALR	0.91	9.64E-126
PA2G4	0.90	6.45E-138
NCL	0.90	6.67E-139
SDF2L1	0.90	1.81E-123
DDX21	0.89	5.77E-148

Figure 3

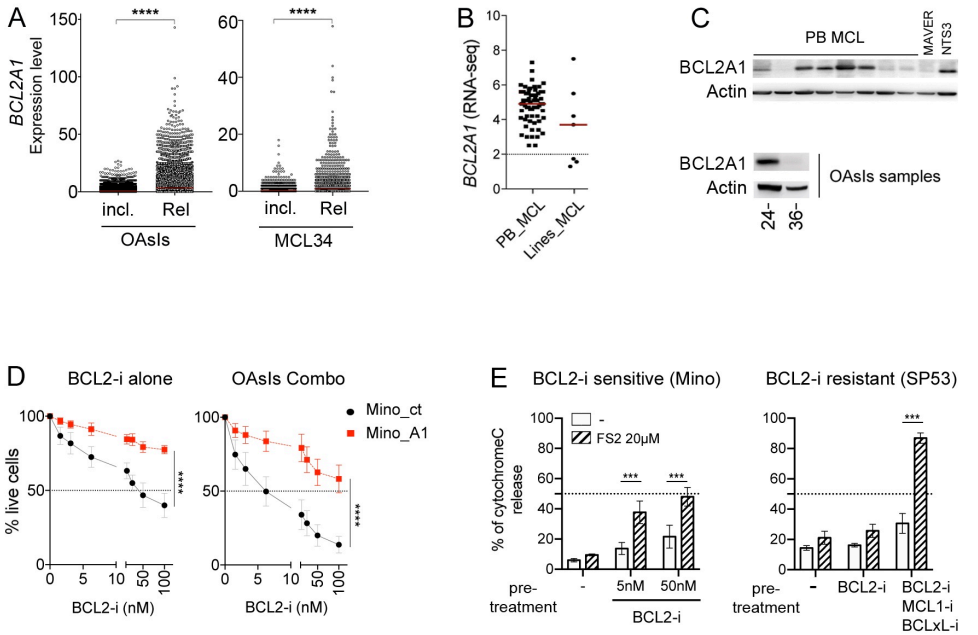
A
BCL2A1
Expression level
150
100
50
0
****
incl.
Rel
OAsIs
60
40
20
0
****
incl.
Rel
MCL34
B
BCL2A1 (RNA-seq)
10
8
6
4
2
0
PB_MCL
Lines_MCL
C
PB MCL
MAVER
NTS3
BCL2A1
Actin
BCL2A1
Actin
OAsIs samples
24-
36-
D
BCL2-i alone
OAsIs Combo
Mino_ct
Mino_A1
% live cells
100
50
0
****
0
5
10
50
100
BCL2-i (nM)
****
E
BCL2-i sensitive (Mino)
BCL2-i resistant (SP53)
% of cytochromeC release
-
FS2 20μM
***
***
***
pre-treatment
-
5nM
50nM
BCL2-i
pre-treatment
-
BCL2-i
BCL2-i
MCL1-i
BCLxL-i

Figure 4

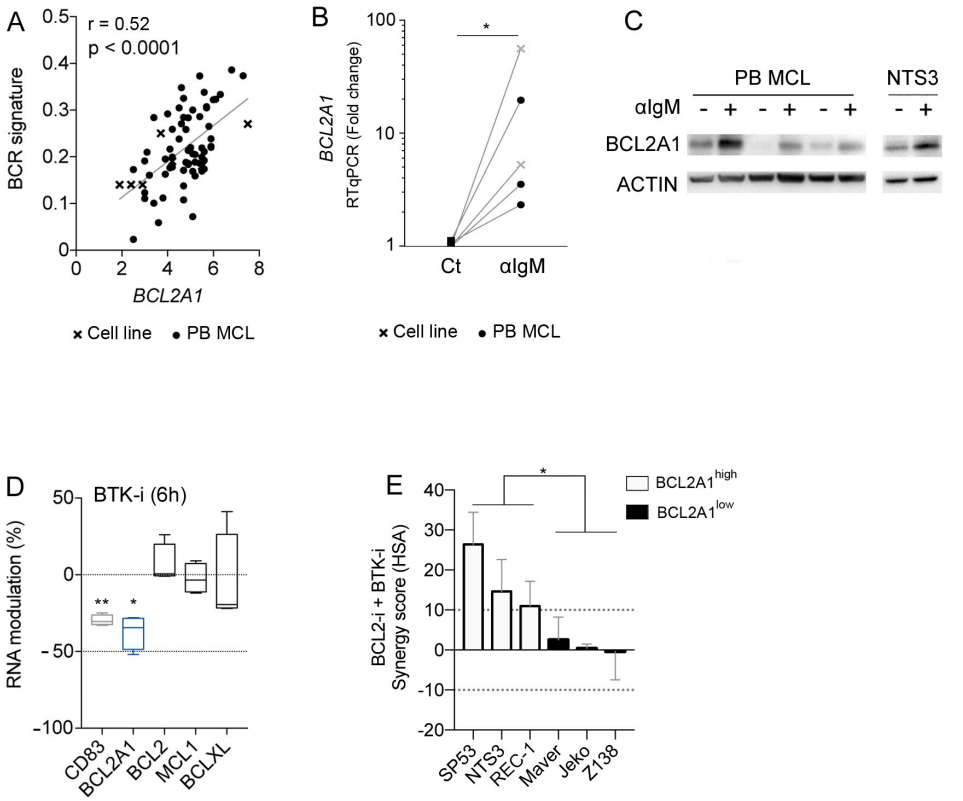
A
r = 0.52
p < 0.0001
BCR signature
BCL2A1
Cell line
PB MCL
B
BCL2A1
RTqPCR (Fold change)
Ct
αIgM
Cell line
PB MCL
C
PB MCL
NTS3
αIgM
BCL2A1
ACTIN
D
BTK-i (6h)
RNA modulation (%)
CD83
BCL2A1
BCL2
MCL1
BCLXL
E
BCL2A1high
BCL2A1low
BCL2-i + BTK-i
Synergy score (HSA)
SP53
NTS3
REC-1
Maver
Jeko
Z138

Figure 5

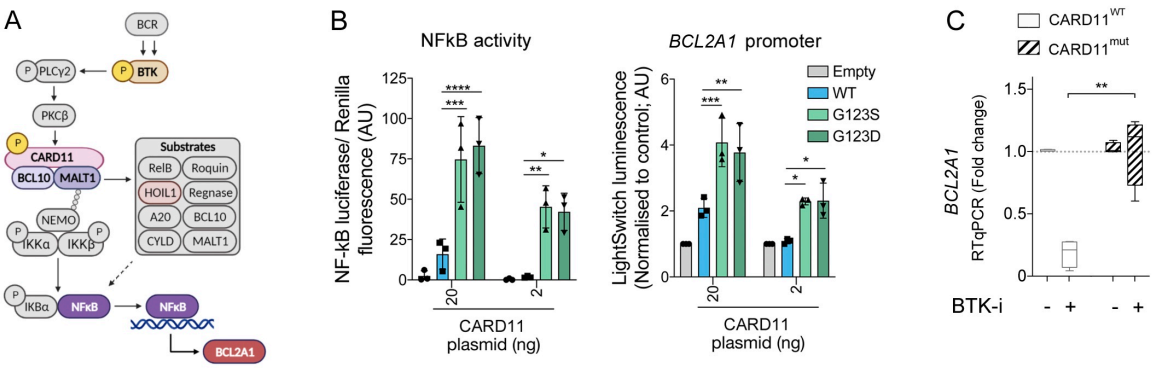
A
BCR
PLCγ2
BTK
PKCβ
CARD11
BCL10
MALT1
NEMO
IKKα
IKKβ
IκBα
NFκB
NFκB
BCL2A1
Substrates
RelB
Roquin
HOIL1
Regnase
A20
BCL10
CYLD
MALT1
B
NFkB activity
NF-kB luciferase/ Renilla fluorescence (AU)
CARD11 plasmid (ng)
BCL2A1 promoter
LightSwitch luminescence (Normalised to control; AU)
Empty
WT
G123S
G123D
C
CARD11WT
CARD11mut
BCL2A1 RTqPCR (Fold change)
BTK-i

Figure 6

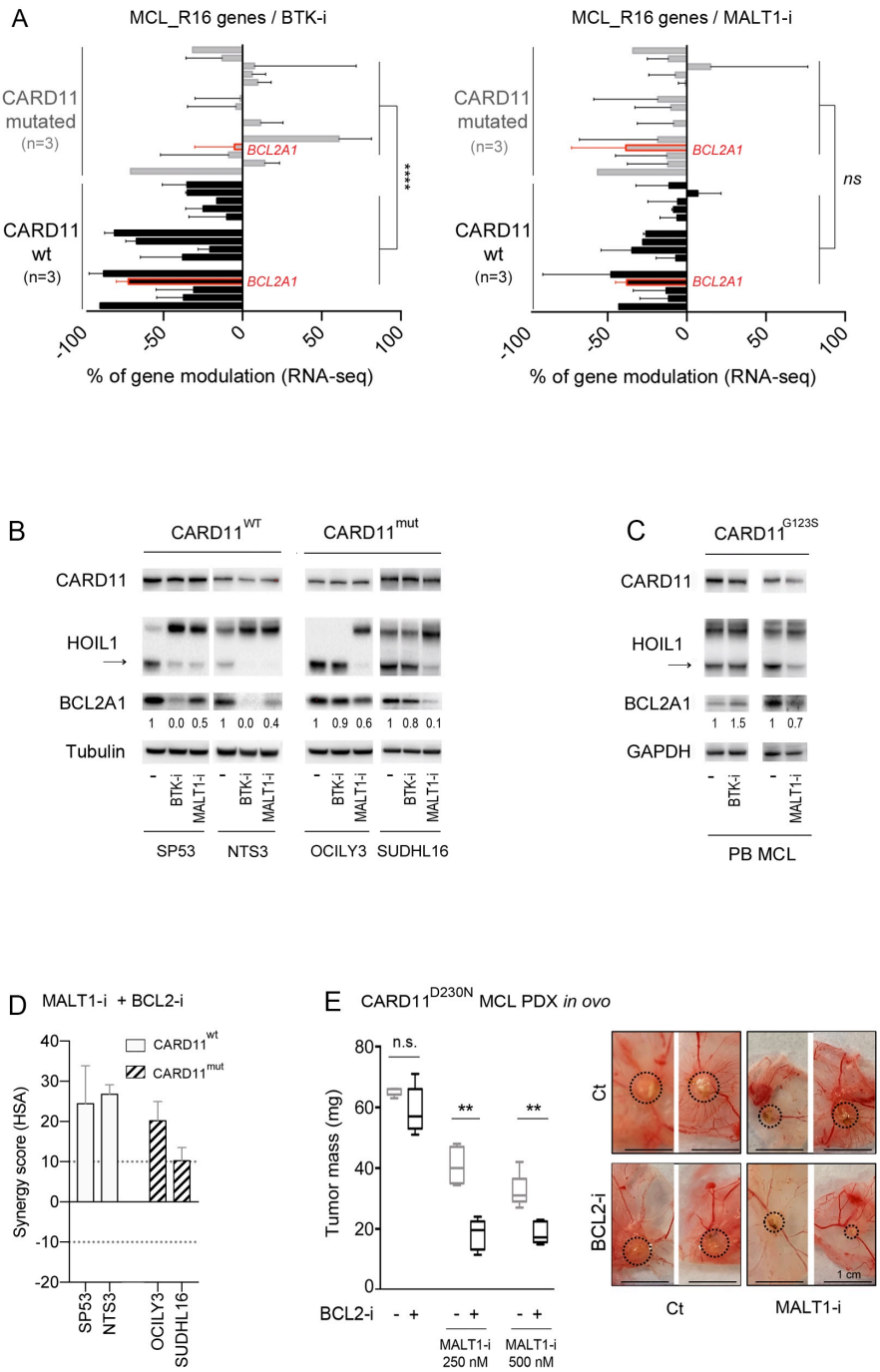
A
MCL_R16 genes / BTK-i
MCL_R16 genes / MALT1-i
CARD11 mutated (n=3)
CARD11 wt (n=3)
BCL2A1
****
ns
-100
-50
0
50
100
% of gene modulation (RNA-seq)
B
CARD11WT
CARD11mut
CARD11
HOIL1
BCL2A1
1 0.0 0.5 1 0.0 0.4 1 0.9 0.6 1 0.8 0.1
Tubulin
- BTK-i MALT1-i
SP53 NTS3 OCILY3 SUDHL16
C
CARD11G123S
1 1.5 1 0.7
GAPDH
PB MCL
D
MALT1-i + BCL2-i
CARD11wt
CARD11mut
Synergy score (HSA)
40
30
20
10
0
-10
-20
SP53 NTS3 OCILY3 SUDHL16
E
CARD11D230N MCL PDX in ovo
n.s.
**
Tumor mass (mg)
80
60
40
20
0
BCL2-i - + - + - +
MALT1-i 250 nM
MALT1-i 500 nM
Ct
BCL2-i
1 cm
Ct
MALT1-i

Figure 7